Regular Paper

Experimental study on the effect of temperature on HDPE geomembrane/geotextile interface shear characteristics

Hai Lin [*], Xiangyu Gong , Yifan Zeng , Chuangbing Zhou

School of Infrastructure Engineering, Nanchang University, 999 Xuefu Avenue, Honggutan District, Nanchang, Jiangxi Province, 330031, China

A B S T R A C T

Geomembranes (GMBs) and geotextiles (GTXs) are the most widely used geosynthetics in landfills and other barrier systems. While various temperature environments may be encountered in practice, the interface shear characteristics of geosynthetics under different temperatures are still not clear. Shear tests of the interface between a high-density polyethylene GMB and nonwoven GTX are performed using a temperature-controlled submerged direct shear apparatus. The testing temperatures range from 10 °C to 70 °C, which covers most of the situations commonly encountered in engineering. The shear behaviors of the textured GMB/GTX interface and smooth GMB/GTX interface are presented, and the mechanism of the temperature influence is analyzed according to the test results and phenomena. Temperature has a significant impact on the GMB/GTX interface peak strength and post-peak strength, and maximum interface shear strength could be obtained when the temperature is approximately 30–40 °C. The influencing mechanisms of temperature on the GMB/GTX interface shear strength are thoroughly discussed. The shear characteristics of the GMB/GTX interface under different temperatures are critical to the stability analysis of geosynthetic slopes in special condition, and this study can also provide a reference for the effect of temperature on the shear behavior of other geosynthetics.

1. Introduction

Geotextiles (GTXs) and geomembranes (GMBs) are the most common geosynthetics, and they are often used together in barrier systems for projects such as non-ferrous metal smelting ponds, municipal solid waste landfills, and water channels (Touze-Foltz et al., 2016; Rowe et al., 2017; Kalpakcı et al., 2018; Rowe and Yu 2019; Shi et al., 2020; Fan and Rowe 2022; Chou et al., 2022). High-density polyethylene (HDPE) GMBs are often used as the main material for impermeable layers owing to their extremely low permeability, and a compacted clay liner or geosynthetic clay liner (GCL) can be combined with the GMB to form a much more effective composite liner system (McCartney et al., 2009; Eid 2011; Yu and Rowe 2018; Li et al., 2020; Abdelaal and Solanki 2022; Lin et al., 2023a; Liu et al., 2023; Eldesouky et al., 2023). Regardless of whether the GTX acts as an independent protection layer or as part of a GCL, there will be direct contact between the GTX and GMB. As a result, the shear strength of the GMB/GTX interface is a key factor for the slope stability (Bergado et al., 2006; Yu and Rowe 2020). Experimental studies on the shear characteristics of GMB/GTX interfaces began in the 1980s, the testing methods (e.g., sample size, shear

rate, hydration state and normal stress) and material properties (e.g., polymer type, texture technology, and fabric) can affect the test results (Mitchell et al., 1990; Stark et al., 1996; Jones and Dixon 1998; Bacas et al., 2015; Feng and Lu 2016; Samanta et al., 2022; Wang et al., 2022).

Geosynthetics may be applied under environments of variable temperature in landfill liners or other engineering barrier systems (Rowe and Hoor 2009; Bouazza et al., 2011; Yesiller et al., 2015; Jafari et al., 2017; Yu and Bathurst 2017; Kumar and Reddy 2021; Kumar et al., 2021). During 10.5 y of monitoring at a landfill site in Philadelphia, the temperature environment of the landfill capping system changes with the season the local seasonal temperature cycle and ranged between 0 °C and 30 °C (Koerner and Koerner 2006). Moreover, degradation of organics and chemical reactions among the landfill waste can cause the temperature to exceed 60 °C (Hanson et al., 2015). The acid-leaching waste soil resulting from the smelting of nonferrous metals such as bauxite and nickel ore can reach a temperature of nearly 100 °C (Stark et al., 2012; Calder and Stark 2010; Martin et al., 2013; Listyarini 2017). In known engineering applications, geosynthetics mostly work in the temperature environment ranges from 10 °C to 70 °C, and special extreme environment may be encountered in the future.

To date, only a few studies have been conducted on the effect of temperature on the interface shear strength of geosynthetics. Akpinar and Benson (2005) conducted shear tests of a GMB/GTX interface at temperatures ranging from 0 to 33 °C. The GMB/GTX interface peak friction angle increased by 2.3°–2.9° as the temperature increased from 0 to 33 °C. Karademir and Frost (2021) carried out shear tests of GMB/GTX interface in a temperature-controlled chamber, and the elevated temperature effects on the GMB/GTX interface shear strength were discussed at a range of ambient temperatures from 21 °C to 50 °C. The tests yielded similar results as Akpinar and Benson (2005) that an increase in temperature increase the GMB/GTX interface shear strength at testing temperatures. However, increasing the temperature led to a marked decrease in the internal shear strength of the needle punched GCL (Bareither et al., 2018; Ghazizadeh and Bareither, 2017, 2018, 2019, 2023; Hou et al., 2023). The shear failure mode changed from fibers pulling out of the GCL GTX side to tensile rupture of the needle-punched fibers, because increasing the temperature results in a reduction in the tensile strength of nonwoven fibers. Moreover, elevated temperature can lead to obvious rise of creep deformation and change of peak shear strength for soil-geosynthetics interfaces (Chao and Fowmes 2021; Chao et al., 2023). Both GMBs and GTXs are thermosensitive polymer materials while the temperature range of existing research on the GMB/GTX interface shear characteristics is not enough, and it is not clear whether the temperature higher than 50 °C will change the GMB/GTX interface shear behavior.

Understanding the mechanism by which temperature influences the GMB/GTX interface characteristics can allow engineers to better assess the stability of slopes employing geosynthetics. However, most previous studies on the shear behaviors of GMB/GTX interfaces have been carried out at room temperature. This study performs shear tests of GMB/GTX interfaces at temperatures ranging from 10 °C to 70 °C, which covers most common situations that may be encountered in landfills. The effect of temperature on the shear characteristics of the GMB/GTX interface is revealed through a comparative analysis of the test results at different temperatures.

2. Experimental program

2.1. Equipment

A self-designed temperature-controlled submerged direct shear apparatus (shown in Fig. 1) was used for the shearing of the GMB/GTX interface. The apparatus can meet the requirements of ASTM D5321M-21 (ASTM, 2021), while achieving submerged shearing and water temperature control functions. The GMB/GTX interface performs lower shear strength in hydration rather than dry state, which make the submerged shear strength more suitable for slope stability analysis. In addition, it is easier to manage the temperature environment in submerged shearing while maintaining a more uniform and stable temperature. The internal dimension of the shear box was a square of 300 mm × 300 mm, and both the upper and lower shear boxes were set in the temperature-controlled water tank. Specimens remained submerged during the entire test process, and the resistance wire was regulated by a computer and thermal sensors to heat device automatically so that the water temperature remains stable throughout the test. A layer of expandable polystyrene (EPS) insulation material was wrapped around the water tank to reduce the heat exchange between the shear apparatus and the environment. Force sensors and displacement sensors were connected to the shear boxes through transmission rods that crossed the top cap or side wall of the water tank. Sealing rings on the transmission rods ensured good water-tightness while the friction force between the connecting rod and the sealing O-ring is too small to have a substantial impact on the testing results. The working temperature range of the sensors is from −20 °C to 80 °C, and little temperature variations were achieved by positioning the sensors outside the shear device. Therefore, the accuracy of the load sensor will not be affected by the testing temperatures. Two needle roller rows were placed between the upper and lower shear boxes to adjust the slit height between the shear boxes and reduce the friction during shearing. A maximum applied stress of 2.2 MPa could be achieved, which can recreate most of the stress state conditions that may be encountered by geosynthetics.

The normal force and shear force were applied through vertical and lateral loading subsystem, respectively. The subsystem was installed in the upper or side space of the mainframe, which was composed of a servo motor with a 24-bit high-precision incremental encoder internally, a reducer, a load sensor, and auxiliary components (Fig. 1). Constant
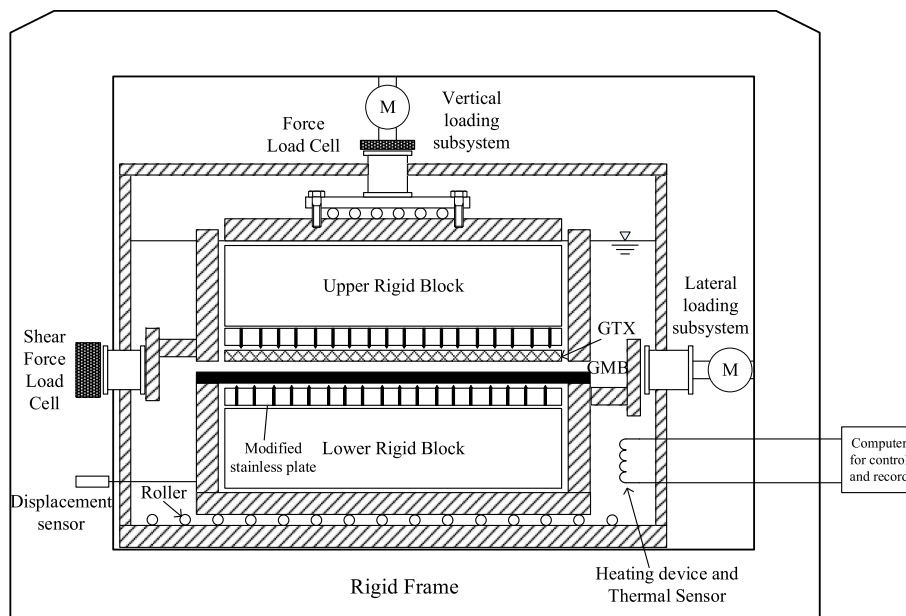

Fig. 1. Temperature-controlled submerged direct shear apparatus.

normal stress and variable shear stress in need as the power source based on computer instructions could be provided by the closed-loop control system composed of a servo motor and a load sensor. The upper shear box was maintained in a fixed position during the shear process, while the lower shear box was driven to move at a constant velocity by the lateral loading subsystem. Rigid rollers were placed at the bottom of the temperature-controlled water tank to reduce the frictional resistance of the apparatus. The maximum lateral shear displacement of the apparatus was approximately 45 mm, and the shear displacement rate could be adjusted in the range of 0.01–10 mm/min. The shear displacement of the specimen, which is identical to that of the lower shear box, was measured by a displacement sensor. For fixation of the GTX and GMB specimens, modified stainless plates were fabricated and positioned in the upper and lower shear boxes (as shown in Fig. 1). The plates have a number of uniformly distributed adjustable-height teeth, formed by installation of nails on each rectangular plate (as shown in Fig. 2), to firmly grip the geosynthetics. The height of the plate sharp teeth could be adjusted from 0 to 1 mm by turning a flat head screw, this allowed a suitable tooth height to be used under different testing normal stress.

2.2. Materials

The GMB and GTX materials used in these tests were provided by a Chinese manufacturer (Changsha Jianyi New Material Co., LTD). The coextruded GMB samples included 2-mm-thick double smooth HDPE GMB and 2-mm-thick and single-sided textured HDPE GMB with asperity height of 0.25 mm. The GTX material was made of needle-punched nonwoven filaments and had a mass per unit area of 300 g/m^2. The physical and mechanical parameters of the geosynthetics used are listed in Table 1 and Table 2.

2.3. Testing methods and procedures

First, the GMB materials were cut into specimens with dimensions of 300×370 mm (corresponding to the outer length of the lower shear box in the shear direction). The GTX material was cut into specimens with dimensions of 300×300 mm (corresponding to the internal dimensions of the shear box). Separate specimens were used for different temperature-normal stress combinations, and each GMB and GTX specimen was cut from the same roll of material, respectively. When

Fig. 2. Modified stainless plates with adjustable-height teeth.

installing the testing specimens in the shear box, the lower rigid block, modified plate with nail teeth, and GMB specimen were placed into the lower shear box sequentially. The nail teeth height of the plate was pre-adjusted according to the testing normal stress to ensure effective surface gripping of the GMB specimen. After the upper shear box was set in place, the GTX specimen was laid on the GMB specimen and covered with the second modified plate followed by the upper rigid block. The upper modified plate was fixed to the stationary upper shear box, and the GTX specimen was gripped firmly to the modified plate. The GMB and GTX specimen showed relatively immobility with the modified plate, which validated good fixation of geosynthetic specimens in all tests. As the length of the GMB specimen along the shear direction was longer than that of the GTX specimen, the problem of area correction during shearing was reasonably avoided. Water was then added to the tank to submerge the GMB and GTX specimens, and a water depth of more than 2 cm was maintained during the entire test procedure. Since water-cooling system was not equipped for the shear apparatus, it is crucial to ensure that the temperature of water added below the target temperature. Adding ice in the water could quickly reduce the water temperature in the tank to below the target testing temperature (e.g., 10 °C), relative stable submerged temperature environment during the entire testing procedure (i.e., lasting no more than 2 h for each test) was confirmed by the records of the thermal sensors. After the tank cover was installed, the displacement sensors were finally set in position.

The load application, temperature control, and data collection were all performed on the control computer during the test. After a normal stress was applied, the water temperature was adjusted to the target value. Based on previous studies (Fox and Stark 2015; Lin et al., 2014, 2018), the shear displacement rate of these tests was set to 1 mm/min to provide comparable results. Based on the possible temperature environment and stress conditions geosynthetic composite liners may encounter, five different temperatures (10, 20, 30, 50, and 70 °C) and five different vertical stress conditions (50, 100, 200, 300, and 400 kPa) were defined. Two repeated shear tests were conducted for the textured GMB/GTX interface and smooth GMB/GTX interface under the condition of $\sigma_n = 50$ kPa and $T = 20$ °C, respectively. The textured GMB/GTX shear results showed that the variability of shear characteristic (i.e., displacement at peak shear stress, peak shear strength, and post peak shear resistance) lied within 2%. The shear force measured by the force sensor has inherent variability which relates to the measurement range of the sensor. The variability of measured shear stress become inapparent with the increase of the normal stress. The smooth GMB performs lower shear strength than the textured GMB, and maximum variability of the interface shear stress is shown for the smooth GMB/GTX interface at $\sigma_n = 50$ kPa. However, the maximum variability remains less than 5%. As the interface shear strength of geosynthetics always show a certain variability (Sia and Dixon 2007), the repeated shear tests could verify that the testing equipment and methods are reasonable and acceptable.

3. Results and analysis

3.1. Stress–displacement relationship

3.1.1. Smooth geomembrane/geotextile interface

The shear stress versus displacement relationship of the smooth GMB/GTX interface under different temperatures is shown in Fig. 3, the results indicate that temperature has a significant influence on the shear stress–displacement curves. When the normal stress is low (i.e., 50 kPa and 100 kPa), no obvious peak stress or post-peak softening phenomena are observed at 10 °C (Fig. 3 a, b). However, obvious peak and post-peak softening phenomena are apparent at temperatures of 20, 30, 50, and 70 °C. Furthermore, the peak shear stress value and post-peak softening extent are related to the temperature, and maximum interface peak strength can be obtained at 30 °C or 40 °C. When the normal stress is greater than 100 kPa, the peak stress and post-peak softening are obvious at the smooth GMB/GTX interface at all testing temperatures (i.
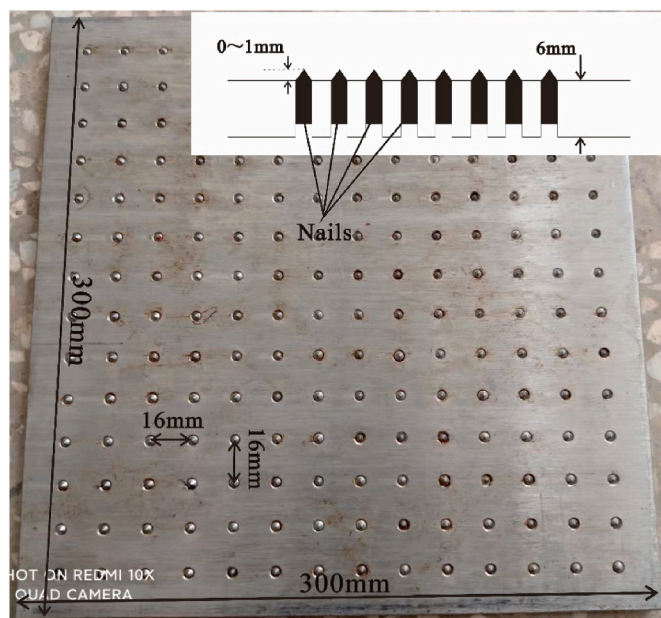
Table 1
Physical and mechanical properties of geomembrane.

Material	Thickness (mm)	Texture height (mm)	Yield strength (N·mm^{-1})	Elongation at yield (%)	Puncture strength (N)	Density (g·cm^{-3})
Textured GMB	2.0	0.25	29	12	534	0.94
Smooth GMB	2.0	0	29	12	640	0.94

Table 2
Physical and mechanical properties of geotextile.

Material	Thickness (mm)	Mass per unit area (g·m^{-2})	Tensile strength (kN·m^{-1})	Elongation (%)	Tear strength (kN)	Puncture strength (kN)
Nonwoven Geotextile	5.5	300	40	75	1.1	7.9

e., 10–70 °C).

Generally, the smooth GMB/GTX interface reaches the peak strength at a small displacement (<4 mm) and a stabilized post-peak shear resistance at a moderate displacement (<10 mm) under all temperature conditions. The very low smooth GMB/GTX interface shear resistance (i. e., 8–27 kPa) at small normal stress (σ_n = 50 kPa) appears almost negligible relative to the measurement range of the shear force sensor (i. e., more than 2 MPa). Apparent variability of measured shear resistance on the shear displacement curve can be observed but remain less than 5%. However, the shear stress variability gradually disappears as the normal stress increases. A slight increase in the post peak shear resistance (<5%) with increasing displacement in case of large displacement can be seen in some of the stress–displacement curves in Fig. 3 (e.g., 40 °C in Fig. 3 d). This phenomenon may be attributed to caused greater roughness on the GMB/GTX due to the vertical deformation of the GMB specimens (Lee and Manjunath 2000; Lashkari and Jamali 2021; Xu et al., 2023). Similar phenomena on the shear stress versus displacement curves can also be seen in literatures (Thielmann et al., 2016; Feng et al., 2022; Liu et al., 2023). However, it does not affect the subsequent analyses while the explanation on this phenomenon still needs further validation.

3.1.2. Textured geomembrane/geotextile interface

The shear stress versus displacement relationships of the textured GMB/GTX interface are shown in Fig. 4. When the normal pressure is low (i.e., σ_n = 50 and 100 kPa), the peak shear stress is not obvious on the stress–displacement curves for the textured GMB/GTX interface at all testing temperatures. However, varying the temperature changes the interface peak shear strength significantly (as shown in Fig. 4 a, b). When the normal stress is higher (e.g., σ_n = 200, 300, and 400 kPa), obvious peak shear stress and post-peak softening can be observed on the textured GMB/GTX shear stress–displacement curves at each temperature. Although the post-peak softening of the textured GMB/GTX interface shear stress-displacement curves differs at different temperatures, it can be seen from Fig. 4 that the stabilized post peak shear resistance can generally be reached when the shear displacement exceeds 30 mm. Combining Figs. 3 and 4, it can be concluded that the temperature has a significant influence on the peak strength and the stabilized post peak shear resistance of the GMB/GTX interface.

The displacement at peak stress (δ_p) of the textured GMB/GTX interface is higher than that of the smooth GMB/GTX interface, which corroborates the results of previous studies (Jones and Dixon 1998; Bacas et al., 2015). The relationship between the displacement at peak stress and the temperature is shown in Fig. 5. Obviously, the exact functional relationship between temperature and δ_p is difficult to derive at present owing to the variability in the GMB/GTX shear results. However, it can be seen from Fig. 5 that δ_p tends to decrease with increasing temperature. In addition, the δ_p values of both the smooth GMB/GTX and textured GMB/GTX interfaces reach a minimum at T = 70 °C.

3.2. Peak shear strength

The relationships between the peak shear strength of the GMB/GTX interface and the temperature under different normal stresses are shown in Fig. 6. The peak strength of the smooth GMB/GTX interface reaches the maximum value at T = 30–40 °C, and the textured GMB/GTX interface peak shear strength reaches the maximum value at T = 30 °C. The magnitude of the change in peak strength with temperature is closely related to the normal stress, and the effect of temperature is generally weaker with increasing normal stress. For example, when the normal stress is low (σ_n = 50 kPa), the peak shear strength of the smooth GMB/GTX interface at T = 10 °C is only 7.7 kPa. The smooth GMB/GTX interface peak shear strength at T = 40 °C is 21.3 kPa, and the ratio of the peak strengths at these two temperatures is 2.8. As the normal stress increases (i.e., to σ_n = 400 kPa), the maximum peak strength ratio decreases to 1.4. The ultimate peak strength ratio of the textured GMB/GTX interface at different temperatures reaches the maximum value 2.1 at σ_n = 100 kPa, and it drops to approximately 1.3 at σ_n = 300–400 kPa. The effect of temperature on the textured GMB/GTX interface peak strength is less than that on the smooth GMB/GTX interface. The shear mechanism of the textured GMB/GTX interface includes interface friction as well as interlocking between the GTX fabric and GMB asperity (Frost and Lee 2001; Hebeler et al., 2005; Li and Gilbert 2006; Vangla and Gali 2016; Araújo et al., 2022; Feng et al., 2022; Lin et al., 2023b). It can be deduced from this phenomenon that the friction and interlocking between the GTX fiber and the GMB surface have different influencing mechanisms at different temperatures.

The peak shear strength parameters of geosynthetic interfaces are often needed for the design of landfills, and the critical strength parameters under the most dangerous conditions help provide a reasonable evaluation of the slope stability of landfill liners. Because the peak shear strength of the hydrated GMB/GTX interface is significantly affected by the temperature, it is necessary to analyze the shear strength parameters at different temperatures. The peak shear strength envelopes of the GMB/GTX interfaces under different temperatures are shown in Fig. 7. Linear envelopes are obtained for the peak strengths under different temperatures in the range of normal stresses in these tests. As the hydrated GMB/GTX interface exhibits very low cohesion, the cohesion parameter is neglected for simplicity in the following analysis. To study the effect of temperature on the peak strength parameters, the derived interface friction angles at different temperatures are summarized in Table 3. The interface friction angles under low and high temperatures are significantly lower than those obtained at T = 30–40 °C. The peak friction angle differences of the smooth GMB/GTX and textured GMB/GTX interfaces are 5.5° and 5.9°, respectively. It can be seen from Fig. 7 and Table 3 that the slope stability may be overestimated if the effect of temperature on the GMB/GTX interface shear strength is ignored, which may cause hidden risks in engineering practice.

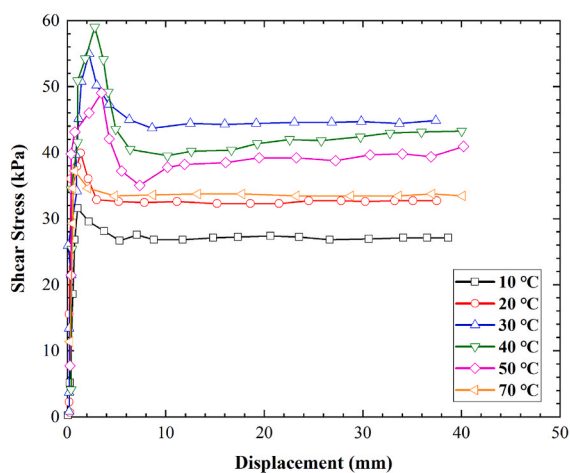*3.3. Post peak shear resistance*

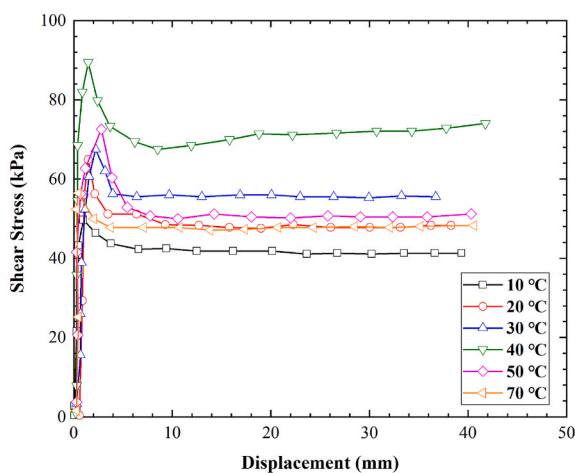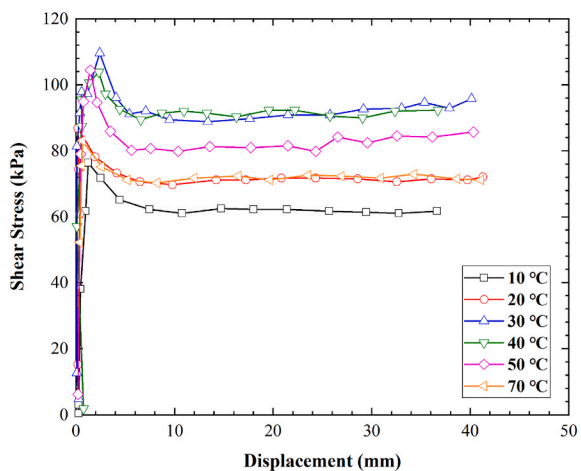The stabilized post peak shear resistance of the GMB/GTX interfaces
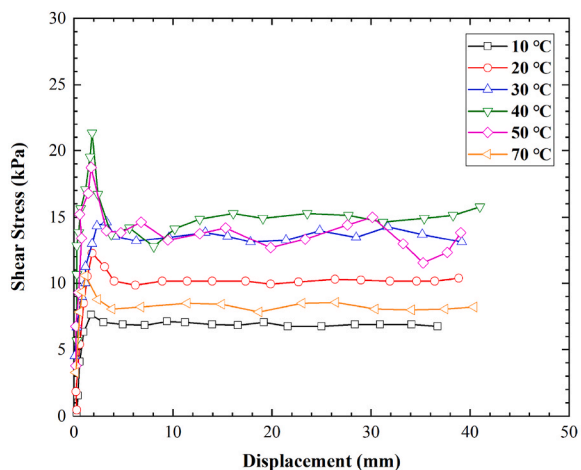
(a) 50 kPa, smooth GMB
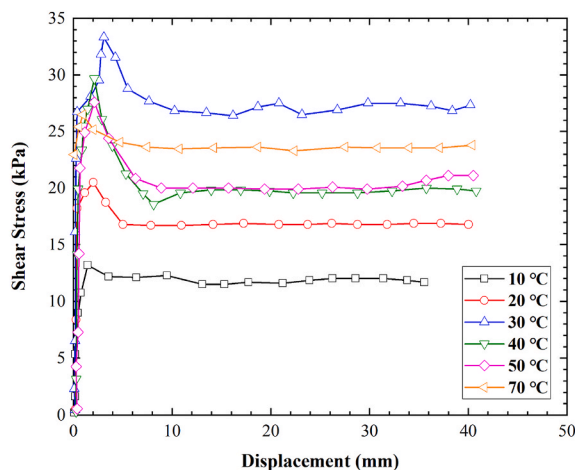
(b) 100 kPa, smooth GMB

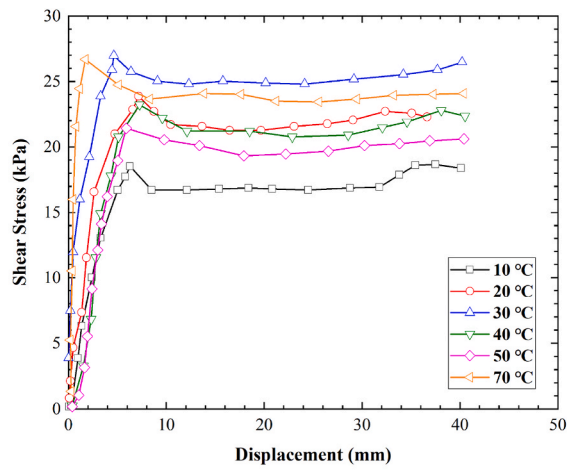(c) 200 kPa, smooth GMB

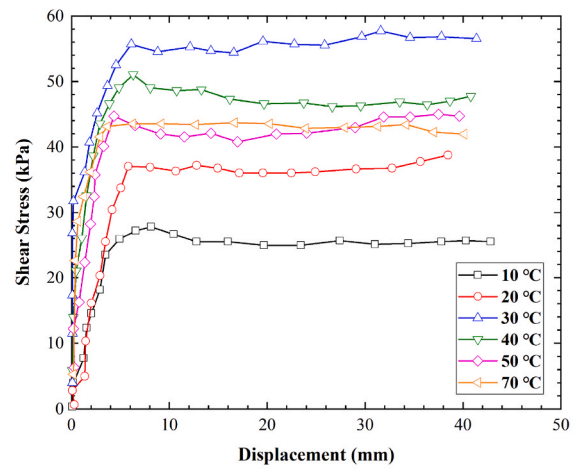(d) 300 kPa, smooth GMB

(e) 400 kPa, smooth GMB

Fig. 3. Shear stress–displacement curves for the smooth GMB/GTX interface.

under different temperatures are shown in Fig. 8. The stabilized post peak shear resistance difference ratios of the textured GMB/GTX and smooth GMB/GTX interfaces are 1.3–2.2 and 1.5–2.3 in the normal stress range of 50–400 kPa, respectively. Similar to the peak shear
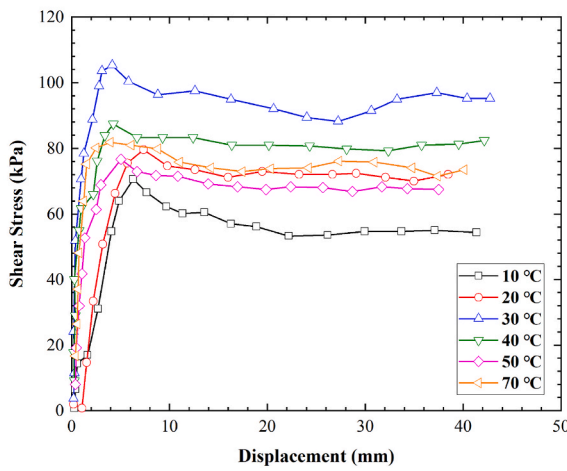
strength, the temperature has a significant effect on the stabilized post peak shear resistance of the GMB/GTX interface. As indicated by Thiel (2001, 2011), Stark and Choi (2004), translational failure is more likely to occur along the interface with lowest peak shear strength. If the
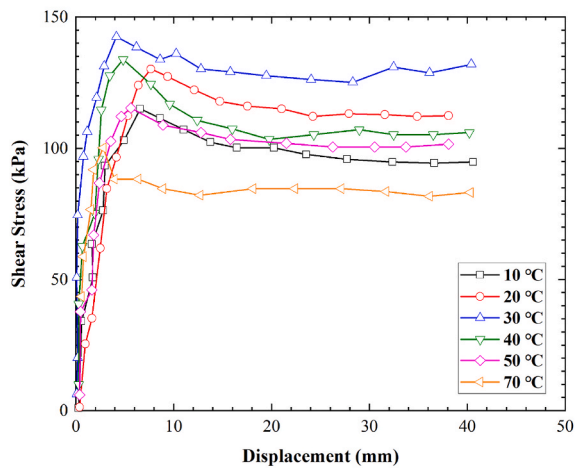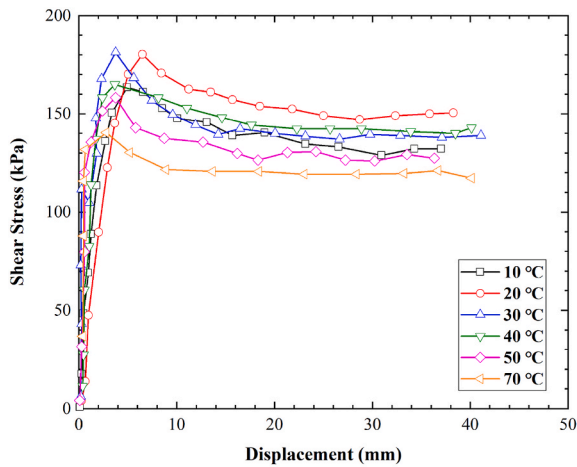
(a) 50 kPa, textured GMB

(b) 100 kPa, textured GMB

(c) 200 kPa, textured GMB

(d) 300 kPa, textured GMB

(e) 400 kPa, textured GMB

Fig. 4. Shear stress–displacement curves for the textured GMB/GTX interface.

GMB/GTX interface behave a potential sliding surface among the multi-layer geosynthetic liner, the effect of temperature on the stabilized post peak shear resistance will play an important role in the stability analysis of landfills. The fitted strength envelopes of the stabilized post peak shear resistance for the GMB/GTX interfaces under different temperatures are shown in Fig. 9, and the strength envelopes remains linear at the different temperatures tested. It can be seen from Fig. 9 and Table 3 that the post-peak strength parameters are affected significantly
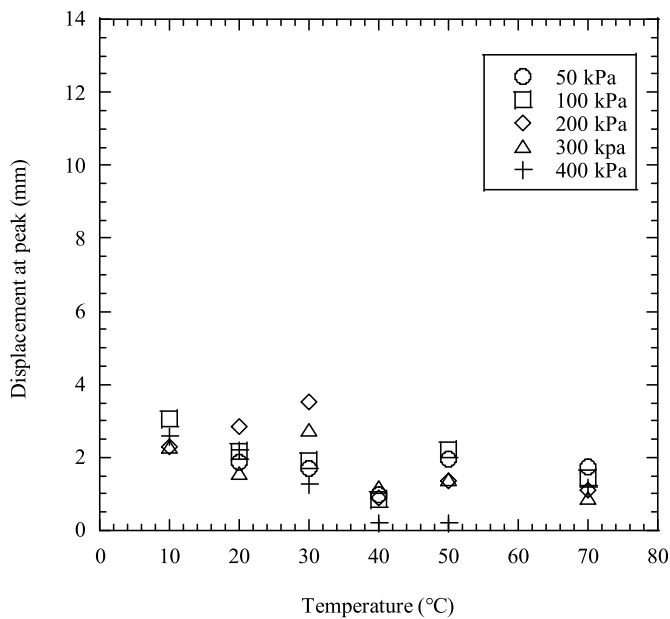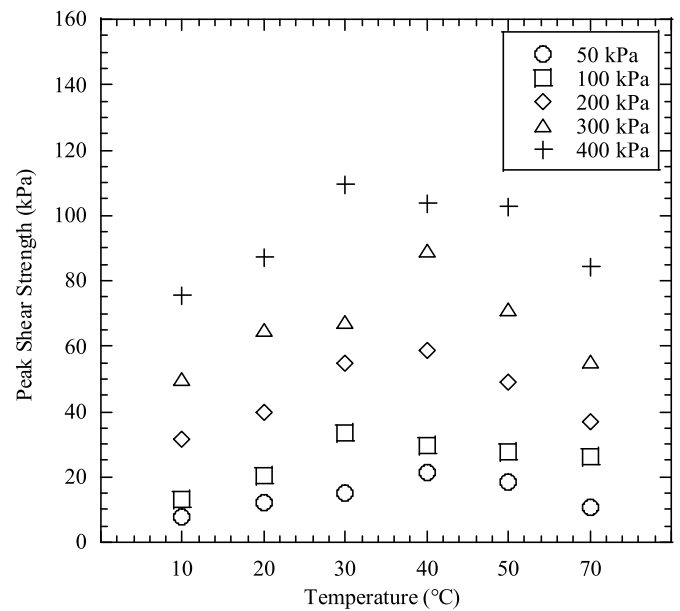
(a) Smooth GMB/GTX interface
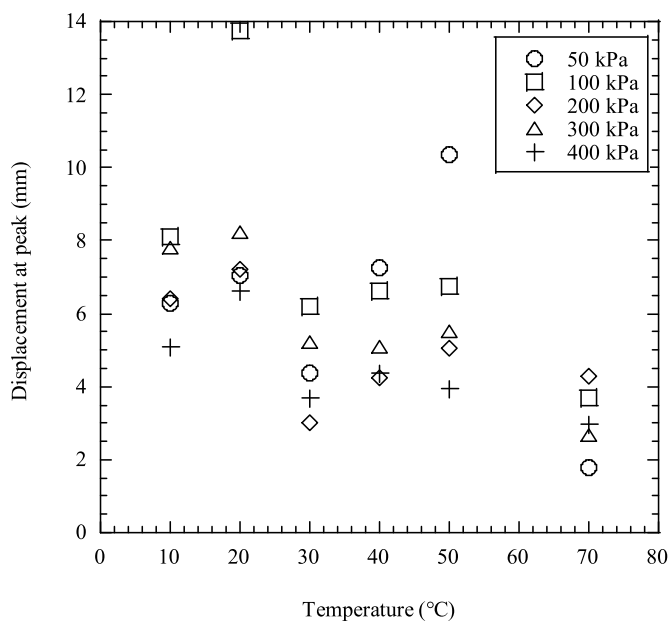
(b) Textured GMB/GTX interface

Fig. 5. Change in the peak displacement with temperature.

(a) Smooth GMB/GTX interface

(b) Textured GMB/GTX interface

Fig. 6. Relationships between peak shear strength and temperature.
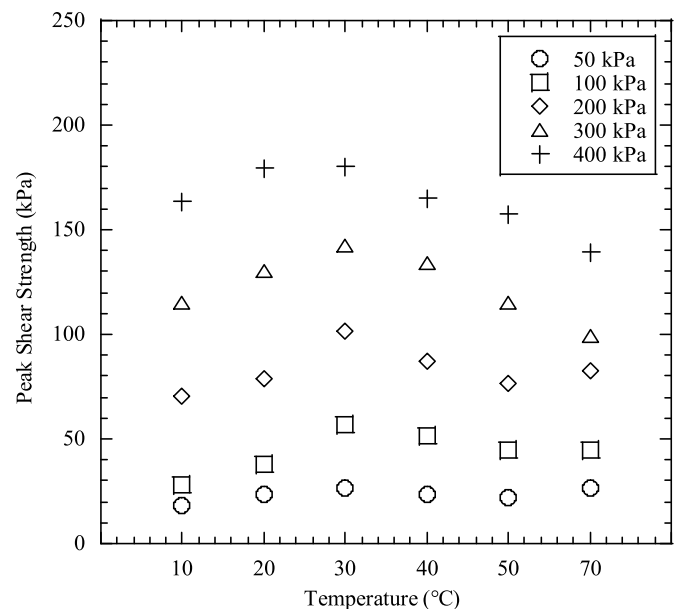
by the temperature, which is similar to the results for the peak strength. Either low (<20 °C) or high (>40 °C) temperatures will significantly reduce the shear strength, and the effect of temperature on the geosynthetic interface shear strength should be considered seriously in the stability analysis of future engineering projects.

4. Mechanism and discussion

The obtained GMB/GTX interface friction angles of peak and post peak shear strength under various temperature conditions are collected and shown in Fig. 10. The results obtained at low temperatures are consistent with previous experimental results, and the results obtained

under high-temperature conditions serve to fill the gaps in the corresponding research. Through the GMB/GTX interface shear tests over a wide normal stress range carried out in this study, it is found that both the peak strength friction angle and post peak strength friction angle initially increase and then decrease with increasing temperature. The interface shear strength friction angle reaches the maximum value at approximately $T = 30$–40 °C. The influence of temperature on the shear strength of the GMB/GTX interface is notable, and thus it cannot be neglected in stability analyses of slopes with geosynthetics. The mechanical properties of the polymer materials are significantly affected by the temperature environment, and the change in surface characteristics of the polymeric materials under different temperatures is a crucial factor affecting the interface shear properties (Frost and Karademir
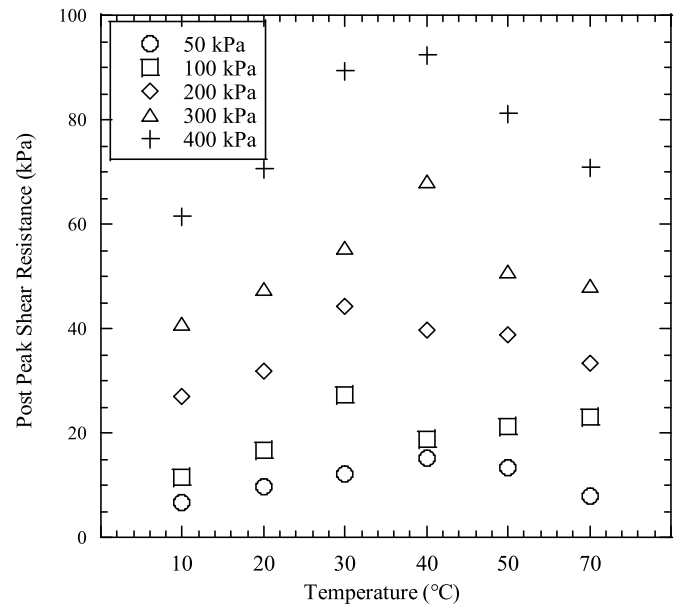
(a) Smooth GMB/GTX interface
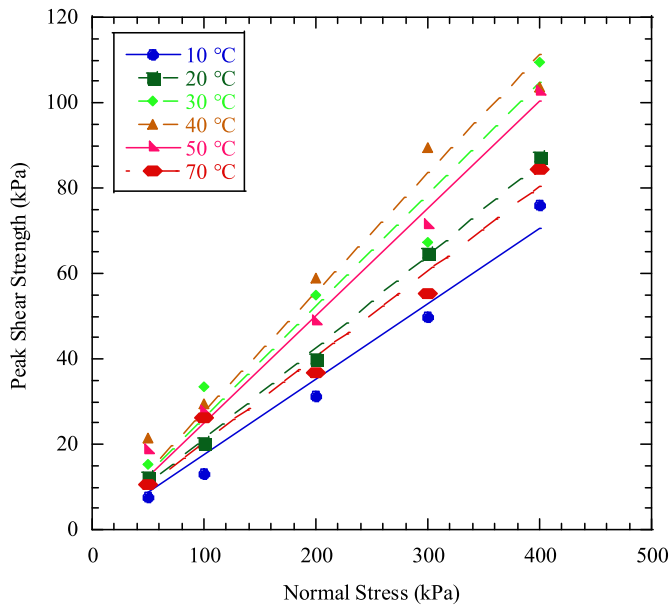
(a) Smooth GM/GT interface
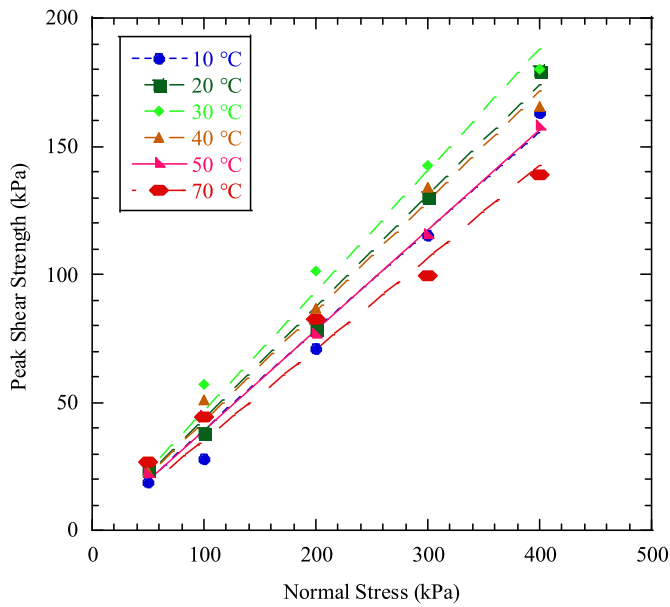
(b) Textured GMB/GTX interface

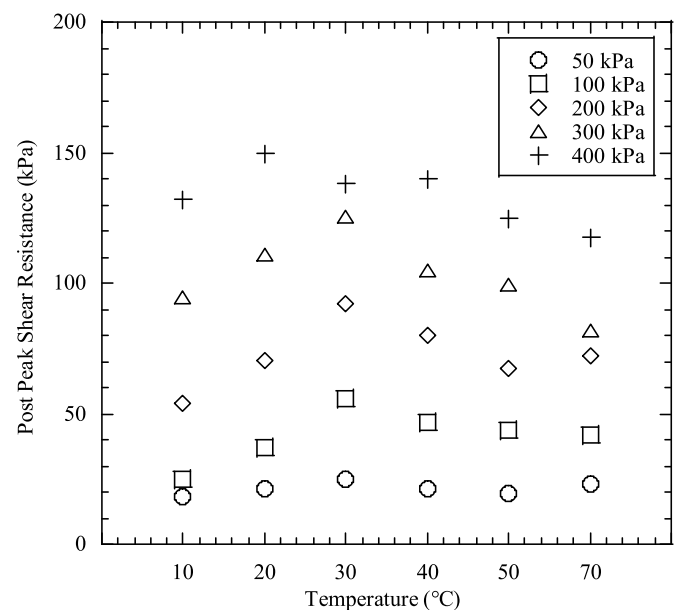**Fig. 7.** Shear peak strength envelopes of GMB/GTX interfaces at different temperatures.
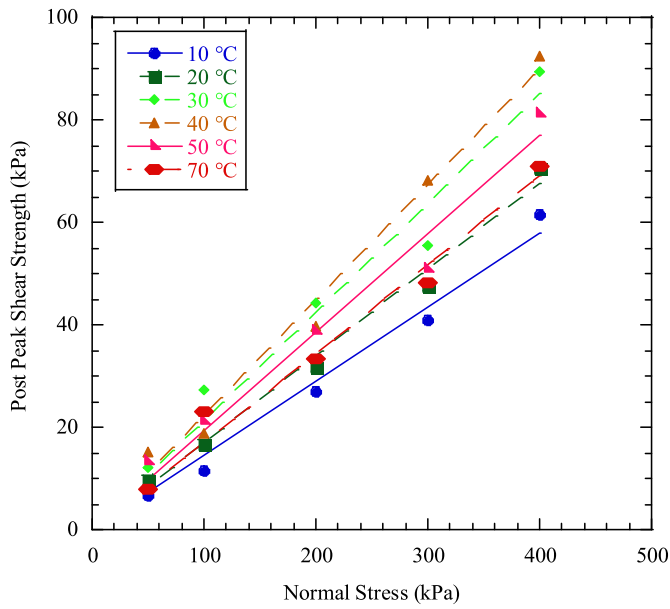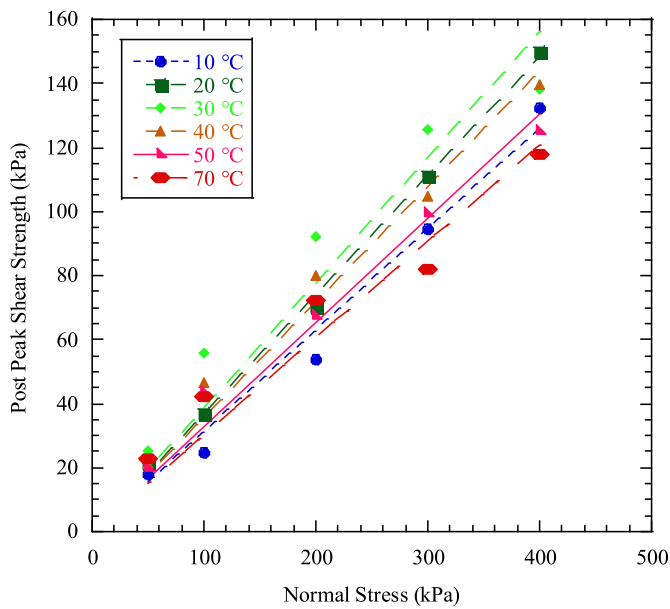

(b) Textured GM/GT interface

Fig. 8. Relationships between the stabilized post peak shear resistance and temperature.

2016).

To analyze the mechanism by which temperature influences the GMB/GTX interface shear strength, standard tensile tests were conducted for GMB specimens (according to ASTM D638-22 (ASTM, 2022)) at different temperatures. The elastic modulus of the GMB specimens at different temperatures are shown in Fig. 11. As the temperature increases from $T = -10\ ^\circ C$ to $T = 90\ ^\circ C$, the material stiffness of the GMB specimens decreases nonlinearly in accordance with the empirical fitting equation shown in Fig. 11. As the elastic modulus of GMB decreases continuously, the shear failure mode of the GMB/GTX interface varies with increasing temperature, resulting in a non-monotonic change of the interface shear resistance. The smooth GMB/GTX interface friction angle

Table 3
Friction angles of GMB/GTX interfaces at different temperatures.

Shear strength parameter	Temperature (°C)					
	10	20	30	40	50	70
Smooth GMB/GTX peak friction angle (°)	10.0	12.1	14.7	15.5	14.1	11.4
Smooth GMB/GTX post peak friction angle (°)	8.2	9.6	12.0	12.7	10.9	9.8
Textured GMB/GTX peak friction angle (°)	21.3	23.5	25.2	23.2	21.4	19.6
Textured GMB/GTX post peak friction angle (°)	17.5	20.4	21.3	19.8	18.1	16.8

(a) Smooth GM/GT interface

(b) Textured GM/GT interface

Fig. 9. Post peak strength envelopes of GMB/GTX interfaces at different temperatures.

increases proportional with the increase of temperature (Fig. 10) when $T < 30$ °C, this may attribute to the increase of interface roughness and actual contact area of geosynthetics by thermal expansion (Vangla and Gali 2016; Lashkari and Jamali 2021; Khan and Latha 2023; Xu et al., 2023). If the surface stiffness of the GMB specimens is low enough, scratches of GTX fibers on the GMB surface will be more easily. Then the shear failure modes can change from surface sliding to fiber plowing as the GMB continues to soften at higher temperatures. As a result, the frictional resistance of the smooth GMM/GTX interface decreases with increasing temperature continuously when $T > 40$ °C.

The shear mechanism of the textured GMB/GTX interface includes friction along with interlocking between the GTX fibers and GMB asperity (Frost and Lee 2001; Hebeler et al., 2005; Li and Gilbert 2006;

de Leeuw et al., 2021; Feng et al., 2022; Lin et al., 2023b). Of the two, the effect of temperature on the friction component can be understood as that of the smooth GMB/GTX interface in the previous paragraph. The difference obtained by the peak strength of the textured GMB/GTX interface subtracting the peak strength of the smooth GMB/GTX interface represents the interlocking effect of the GMB asperity. Considering that the surface cohesion of the GMB/GTX interface can be neglected (Fig. 9), the interlocking component of the textured GMB/GTX interface at different temperatures can be represented by the friction angle difference between textured GMB/GTX interface and smooth GMB interface. The relationship between the asperity interlocking component of the textured GMB interface shear strength and the temperature is shown in Fig. 12. The interlocking component remains stable at $T = 10$–30 °C, but it decreases significantly to another stabilized value when the temperature is between 40 °C and 60 °C. This indicates that the mechanical failure mechanism of the asperity interlocking effect changes at $T > 40$ °C. The scratch strength of GTX fiber on HDPE material decreases at high temperatures, which may cause the interlocking component to be determined by GMB asperity cut by GTX fiber rather than surrounding pulling of fibers. Since the asperity interlocking can be weakened at relatively high temperatures ($T > 40$ °C), more severe reduction in the shear strength will occur for the textured GMB/GTX interface compared with that for the smooth GMB/GTX interface. However, the asperity interlocking effect no longer changes significantly when the temperature is further increased.

The material surfaces after textured GMB/GTX interface shearing at $\sigma_n = 400$ kPa under $T = 30$ °C and $T = 70$ °C are shown in Fig. 13. The GTX fibers are pulled at the surface under both temperatures, but the GTX surface appears softer and larger fiber deformation under $T = 70$ °C. The textured GMB surface does not change significantly after shearing at $T = 30$ °C, and it can be deduced that the interlocking component mainly depends on the pulling of fibers around the GMB asperity in this case. After shearing at $T = 70$ °C, the roughness of the textured GMB surface is reduced obviously in height, and it is found that many GMB asperity are pulled and cut into planes by the GTX fibers. This phenomenon further demonstrates that the mechanical mechanism of the interlocking effect changes from the surrounding pulling mode under low temperatures to a cutting mode under high temperatures, which verifies the hypothesis of interface shear failure mode transition. The above analysis can explain why the GMB/GTX interface shear strength changes with temperature.

5. Conclusion

Shear tests of the smooth geomembrane (GMB)/geotextile (GTX) interface and textured GMB/GTX interface are conducted at temperatures ranging from 10 to 70 °C using a temperature-controlled submerged shear apparatus. The GMB/GTX interface shear characteristics under different temperatures are exhibited, and the effect of temperature on the interface shear strength is elucidated. Through comparative analysis of the test results and phenomena, the mechanisms by which temperature influences the shear strength of the GMB/GTX interface are revealed. The main conclusions are as follows.

(1) The temperature change does not alter the shear stress displacement curve trend of either the smooth GMB/GTX or the textured GMB/GTX interfaces. The shear displacement at the peak exhibits a certain variability under different temperatures for both the smooth GMB/GTX and textured GMB/GTX interfaces. However, the displacement required for the GMB/GTX interface to reach peak strength decreases with increasing temperature in overall trend.

(2) The temperature has a significant impact on the GMB/GTX interface peak strength and post peak shear resistance. The shear strength envelopes at normal stresses ranging from 50 to 400 kPa are all linear under different temperatures. The shear strength of the smooth GMB/GTX and textured GMB/GTX interfaces reach a
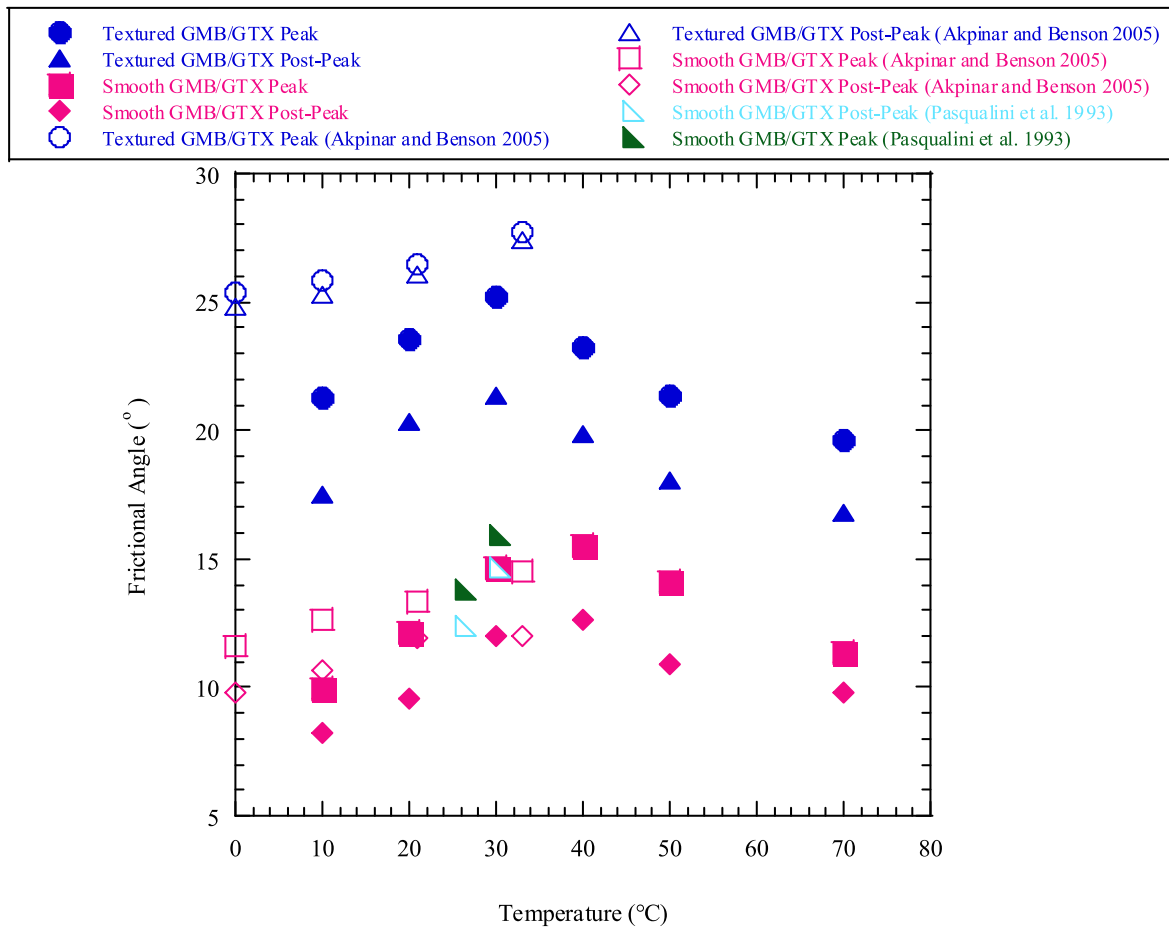
Fig. 10. Shear friction angles of the GM/GT interfaces at different temperatures.
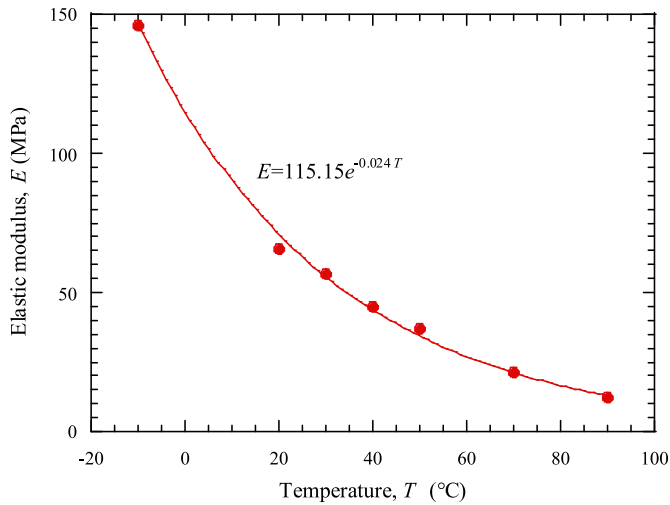

Fig. 11. Elastic modulus of the geomembrane at different temperatures.
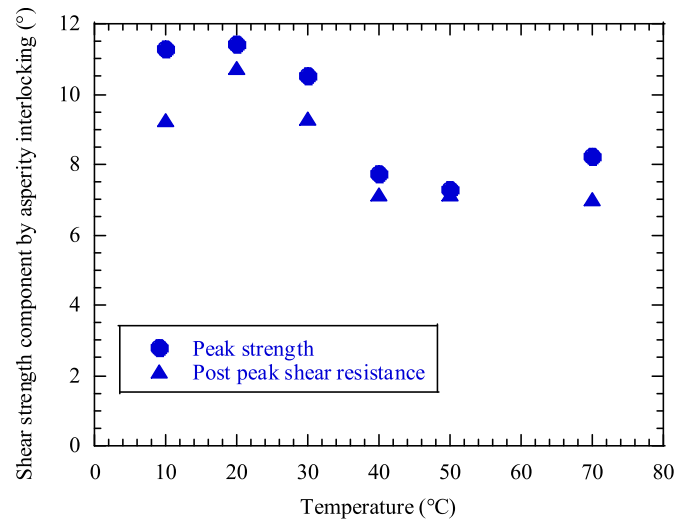

Fig. 12. Influence of temperature on the asperity interlocking component of the shear strength.

maximum value when the temperature is approximately 30–40 °C. Increasing or decreasing the temperature will significantly reduce the GMB/GTX interface shear strength. The peak strength difference ratio under different temperatures ranges from 1.3 to 2.8, and the stabilized post peak shear resistance difference ratio ranges from 1.3 to 2.3.

(3) The interface cohesion of the GMB/GTX interface is small, and the interface shear strength can thus be represented by the

interface friction angle parameter. The peak (post peak) friction angle of the textured GMB/GTX interface is 25.2° (21.3°) at $T = 30$ °C, and the peak (post peak) friction angle decreases to 19.6° (16.8°) at $T = 70$ °C. The peak (post peak) friction angle of the smooth GMB/GTX interface is 15.5° (21.3°) at $T = 40$ °C, and the friction angle decreases to 12.7° (8.2°) at $T = 10$ °C.
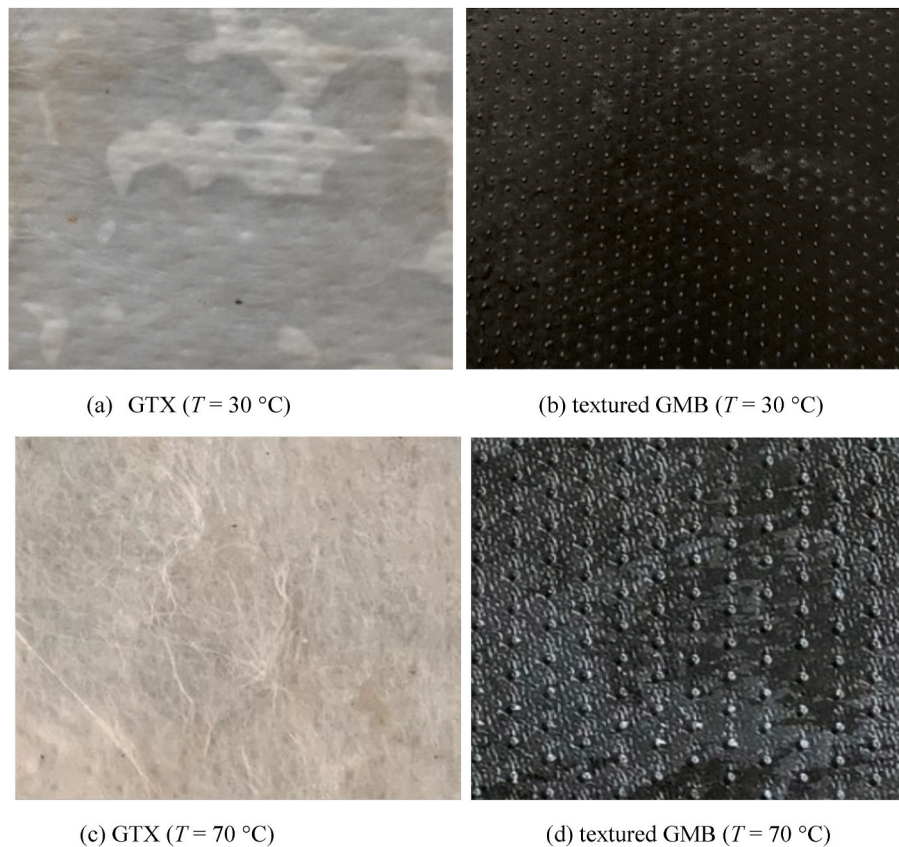
(a) GTX (T = 30 °C)

(b) textured GMB (T = 30 °C)

(c) GTX (T = 70 °C)

(d) textured GMB (T = 70 °C)

Fig. 13. Surfaces of the textured GMB/GTX interface after shearing.

(4) The mechanism of the temperature influencing the textured GMB/GTX interface includes two components, friction as well as interlocking between asperity and GTX fibers. The change in the shear strength of the smooth GMB/GTX interface under different temperatures represents the effect of temperature on the material friction. The interlocking between the GMB asperity and GTX fibers does not perform sensitive changes with temperatures. However, a sudden change in the GMB asperity interlocking effect occurs at approximately T = 40 °C because the shear failure of the textured GMB/GTX interface changes from surrounding pulling mode under low temperatures to cutting mode under higher temperatures.

CRediT authorship contribution statement

Hai Lin: Writing – review & editing, Writing – original draft, Validation, Methodology, Funding acquisition, Conceptualization. **Xiangyu Gong:** Writing – original draft, Visualization, Investigation. **Yifan Zeng:** Writing – original draft, Validation, Investigation, Formal analysis, Data curation. **Chuangbing Zhou:** Writing – review & editing, Supervision, Methodology, Conceptualization.

Data availability

Data will be made available on request.

References

Abdelaal, F.B., Solanki, R., 2022. Effect of geotextile ageing and geomembrane surface roughness on the geomembrane-geotextile interfaces for heap leaching applications. Geotext. Geomembranes 50 (1), 55–68.

Akpinar, M.V., Benson, C.H., 2005. Effect of temperature on shear strength of two geomembrane-geotextile interfaces. Geotext. Geomembranes 23 (5), 443–453.

Araújo, G.L.S., Sánchez, N.P., Palmeira, E.M., de Almeida, M.G.G., 2022. Influence of micro and macroroughness of geomembrane surfaces on soil-geomembrane and geotextile-geomembrane interface strength. Geotext. Geomembranes 50 (4), 751–763.

ASTM, 2021. Standard Test Method for Determining the Shear Strength of Soil-Geosynthetic and Geosynthetic-Geosynthetic Interfaces by Direct Shear. Annual Book of ASTM Standards. ASTM D5321, West Conshohocken, PA.

ASTM, 2022. Standard Test Method for Tensile Properties of Plastics. Annual Book of ASTM Standards. ASTM D638, West Conshohocken, PA.

Bacas, B.M., Cañizal, J., Konietzky, H., 2015. Shear strength behavior of geotextile/geomembrane interfaces. J. Rock Mech. Geotech. Eng. 7 (6), 638–645.

Bareither, C.A., Soleimanian, M., Ghazizadeh, S., 2018. Direct shear testing of GCLs at elevated temperature and in a non-standard solution. Geosynth. Int. 25 (3), 350–368.

Bergado, D.T., Ramana, G.V., Sia, H.I., Varun, 2006. Evaluation of interface shear strength of composite liner system and stability analysis for a landfill lining system in Thailand. Geotext. Geomembranes 24 (6), 371–393.

Bouazza, A., Nahlawi, H., Aylward, M., 2011. In situ temperature monitoring in an organic-waste landfill cell. J. Geotech. Geoenviron. Eng. 137 (12), 1286–1289.

Calder, G.V., Stark, T.D., 2010. Aluminum reactions and problems in municipal solid waste landfills. Pract. Period. Hazard. Toxic, Radioact. Waste Manag. 14 (4), 258–265.

Chao, Z., Fowmes, G., 2021. Modified stress and temperature-controlled direct shear apparatus on soil-geosynthetics interfaces. Geotext. Geomembranes 49 (3), 825–841.

Chao, Z., Shi, D., Fowmes, G., Xu, X., Yue, W., Cui, P., Hu, T., Yang, C., 2023. Artificial intelligence algorithms for predicting peak shear strength of clayey soil-geomembrane interfaces and experimental validation. Geotext. Geomembranes 51 (1), 179–198.

Chou, Y.C., Brachman, R.W.I., Rowe, R.K., 2022. Leakage through a hole in a geomembrane beneath a fine-grained tailings. Can. Geotech. J. 59 (3), 372–383.

de Leeuw, L.W., Dietz, M.S., Milewski, H., Mylonakis, G., Diambra, A., 2021. Relationship between texture of polypropylene coatings and interface friction for sand at low stress levels. Can. Geotech. J. 58 (12), 1884–1897.

Eid, H.T., 2011. Shear strength of geosynthetic composite systems for design of landfill liner and cover slopes. Geotext. Geomembranes 29 (3), 335–344.

Eldesouky, H.M.G., Thiel, R., Brachman, R.W.I., 2023. Assessment of geomembrane strain from pond liner bubbles. Geotext. Geomembranes 51 (6), 28–40.

Fan, J., Rowe, R.K., 2022. Seepage through a circular geomembrane hole when covered by fine-grained tailings under filter incompatible conditions. Can. Geotech. J. 59 (3), 410–423.

Feng, S.J., Lu, S.F., 2016. Repeated shear behaviors of geotextile/geomembrane and geomembrane/clay interfaces. Environ. Earth Sci. 75 (3), 273.

Feng, S.J., Wang, Y.Q., Chen, H.X., 2022. DEM simulation of geotextile-geomembrane interface direct shear test considering the interlocking and wearing processes. Comput. Geotech. 148, 104805.

Fox, P.J., Stark, T.D., 2015. State-of-the-art report: GCL shear strength and its measurement– ten-year update. Geosynth. Int 22 (1), 3–47.

Frost, J.D., Karademir, T., 2016. Shear-induced changes in smooth geomembrane surface topography at different ambient temperatures. Geosynth. Int 23 (2), 113–128.

Frost, J.D., Lee, S.W., 2001. Microscale study of geomembrane-geotextile interactions. Geosynth. Int 8 (6), 577–597.

Ghazizadeh, S., Bareither, C.A., 2017. Temperature-Dependent shear behavior of geosynthetic clay liners. Geotechnical Frontiers 280 (3), 288–298.

Ghazizadeh, S., Bareither, C.A., 2018. Stress-controlled direct shear testing of geosynthetic clay liners II: assessment of shear behavior. Geotext. Geomembranes 46 (5), 667–677.

Ghazizadeh, S., Bareither, C.A., 2019. Temperature effects on inter shear behavior in reinforced GCLs. J. Geotech. Geoenviron. Eng. 146 (1), 04019124.

Ghazizadeh, S., Bareither, C.A., 2023. Effect of temperature on critical strength of geosynthetic clay liner/textured geomembrane composite systems. Geotext. Geomembranes (in press).

Hanson, J.L., Chrysovergis, T.S., Yesiller, N., Manheim, D.C., 2015. Temperature and moisture effects on GCL and textured geomembrane interface shear strength. Geosynth. Int 22 (1), 110–124.

Hebeler, G.L., Frost, J.D., Myers, A.T., 2005. Quantifying hook and loop interaction in textured geomembrane-geotextile systems. Geotext. Geomembranes 23 (1), 77–105.

Hou, J., Xing, X., Benson, C.H., 2023. Thermo-hydro-mechanical shear behavior of interfaces between a textured geomembrane and geosynthetic clay liner. In: Geo-Congress 2023. American Society of Civil Engineers, Reston VA, pp. 545–553.

Jafari, N.H., Stark, T.D., Thalhamer, T., 2017. Spatial and temporal characteristics of elevated temperatures in municipal solid waste landfills. Waste Manag. 59 (1), 286–301.

Jones, D.R.V., Dixon, N., 1998. Shear strength properties of geomembrane/geotextile interfaces. Geotext. Geomembranes 16 (1), 45–71.

Kalpakcı, V., Bonab, A.T., Özkan, M.Y., Gülerce, Z., 2018. Experimental evaluation of geomembrane/geotextile interface as base isolating system. Geosynth. Int 25 (1), 1–11.

Karademir, T., Frost, J.D., 2021. Elevated temperature effects on geotextile-geomembrane interface shear behavior. J. Geotech. Geoenviron. Eng. 147 (12), 04021148.

Khan, R., Latha, G.M., 2023. Multi-scale understanding of sand-geosynthetic interface shear response through Micro-CT and shear band analysis. Geotext. Geomembranes 51 (3), 437–453.

Koerner, G.R., Koerner, R.M., 2006. Long-term temperature monitoring of geomembranes at dry and wet landfills. Geotext. Geomembranes 24 (1), 72–77.

Kumar, G., Kopp, K.B., Reddy, K.R., Hanson, J.L., Yeşiller, N., 2021. Influence of waste temperatures on long-term landfill performance: coupled numerical modeling. J. Environ. Eng. 147 (3), 04020158.

Kumar, G., Reddy, K.R., 2021. Comprehensive coupled thermo-hydro-bio-mechanical model for holistic performance assessment of municipal solid waste landfills. Comput. Geotech. 132, 103920.

Lashkari, A., Jamali, V., 2021. Global and local sand-geosynthetic interface behaviour. Geotechnique 71 (4), 346–367.

Lee, K.M., Manjunath, V.R., 2000. Soil-geotextile interface friction by direct shear tests. Can. Geotech. J. 37 (1), 238–252.

Li, L., Fall, M., Fang, K., 2020. Shear behavior at interface between compacted clay liner-geomembrane under freeze-thaw cycles. Cold Reg. Sci. Technol. 172, 103006.

Li, M.H., Gilbert, R.B., 2006. Mechanism of post-peak strength reduction for textured geomembrane-nonwoven geotextile interfaces. Geosynth. Int 13 (5), 206–209.

Lin, H., Huang, W., Wang, L., Liu, Z., 2023a. Transport of organic contaminants in composite vertical cut-off wall with defective HDPE geomembrane. Polymers 15 (14), 3031.

Lin, H., Shi, J., Qian, X., Zhang, L., 2014. An improved simple shear apparatus for GCL internal and interface stress-displacement measurements. Environ. Earth Sci. 71 (8), 3761–3771.

Lin, H., Zhang, L., Xiong, Y., 2018. Research on shear strength of needle-punched GCL by simple-shear of composite liner. Eng. Geol. 244, 86–95.

Lin, J., Stark, T.D., Idries, A., Choi, S., 2023b. GMX/GDC strength loss mechanisms. Geosynth. Int 1–11.

Listyarini, S., 2017. Designing heap leaching for nickel production that environmentally and economically sustain. Int. J. Environ. Sustain Dev. 8 (12), 799–803.

Liu, Z., Shi, J., Lin, H., Zhang, Y., 2023. Strength characteristics of smooth HDPE geomembrane/nonwoven geotextile interface based on a novel ring shear apparatus. Polymers 15 (11), 2497.

Martin, J.W., Stark, T.D., Thalhamer, T., Gerbasi-Graf, G.T., Gortner, R.E., 2013. Detection of aluminum waste reactions and waste fires. Journal of Hazardous, Toxic, and Radioactive Waste 17 (3), 164–174.

McCartney, J.S., Zornberg, J.G., Swan Jr., R.H., 2009. Analysis of a large database of GCL-geomembrane interface shear strength results. J. Geotech. Geoenviron. Eng. 135 (2), 209–223.

Mitchell, J.K., Seed, R.B., Seed, H.B., 1990. Kettleman hills waste landfill slope failure I: liner-system properties. Journal of geotechnical engineering 116 (4), 647–668.

Rowe, R.K., Hoor, A., 2009. Predicted temperatures and service lives of secondary geomembrane landfill liners. Geosynth. Int 16 (2), 71–82.

Rowe, R.K., Joshi, P., Brachman, R.W.I., McLeod, H., 2017. Leakage through holes in geomembranes below saturated tailings. J. Geotech. Geoenviron. Eng. 143 (2), 04016099.

Rowe, R.K., Yu, Y., 2019. Magnitude and significance of tensile strains in geomembrane landfill liners. Geotext. Geomembranes 47 (3), 439–458.

Samanta, M., Bhowmik, R., Khanderi, H., 2022. Laboratory evaluation of dynamic shear response of sand - geomembrane interface. Geosynth. Int 29 (1), 99–112.

Shi, J., Shu, S., Qian, X., Wang, Y., 2020. Shear strength of landfill liner interface in the case of varying normal stress. Geotext. Geomembranes 48 (5), 713–723.

Sia, A.H.I., Dixon, N., 2007. Distribution and variability of interface shear strength and derived parameters. Geotext. Geomembranes 25 (3), 139–154.

Stark, T.D., Choi, H., 2004. Peak versus residual interface strengths for landfill liner and cover design. Geosynth. Int 11 (6), 491–498.

Stark, T.D., Martin, J.W., Gerbasi, G.T., Thalhamer, T., Gortner, R.E., 2012. Aluminum waste reaction indicators in a municipal solid waste landfill. J. Geotech. Geoenviron. Eng. 138 (3), 252–261.

Stark, T.D., Williamson, T.A., Eid, H.T., 1996. HDPE geomembrane/geotextile interface shear strength. Journal of Geotechnical Engineering 122 (3), 197–203.

Thielmann, S.S., Fox, P.J., Athanassopoulos, C., 2016. Shear strength of GMX/GCL composite liner under high normal stress. J. Geotech. Geoenviron. Eng. 142 (5), 04016005.

Thiel, R., 2001. Peak vs. residual shear strength for landfill bottom liner stability analyses. Proceedings of the 15th Annual GRI Conference Hot Topics in Geosynthetics – II, pp. 40–70. Houston, Texas, USA.

Thiel, R., 2011. Discussion of "Modification to translational failure analysis of landfills incorporating seismicity". J. Geotech. Geoenviron. Eng. 137 (12), 1299–1300.

Touze-Foltz, N., Bannour, H., Barral, C., Stoltz, G., 2016. A review of the performance of geosynthetics for environmental protection. Geotext. Geomembranes 44 (5), 656–672.

Vangla, P., Gali, M.L., 2016. Shear behavior of sand-smooth geomembrane interfaces through micro-topographical analysis. Geotext. Geomembranes 44 (4), 592–603.

Wang, H., Feng, S., Shen, Y., Chang, J., 2022. Experimental investigation on the shear characteristics and failure mechanism between geomembrane/geotextile interfaces. J. Test. Eval. 50 (4), 2083–2102.

Xu, G., Shi, J., Li, Y., 2023. Change pattern of geomembrane surface roughness for geotextile/textured geomembrane interfaces. Geotext. Geomembranes 51 (1), 88–99.

Yesiller, N., Hanson, J.L., Yee, E.H., 2015. Waste heat generation: a comprehensive review. Waste Manag. 42 (5), 166–179.

Yu, Y., Bathurst, R.J., 2017. Modelling of geosynthetic-reinforced column-supported embankments using 2D full-width model and modified unit cell approach. Geotext. Geomembranes 45 (2), 103–120.

Yu, Y., Rowe, R.K., 2018. Development of geomembrane strains in waste containment facility liners with waste settlement. Geotext. Geomembranes 46 (2), 226–242.

Yu, Y., Rowe, R.K., 2020. Geosynthetic integrity and stability analysis for a waste containment facility with a preferential slip plane within the liner system. Geotext. Geomembranes 48 (5), 634–646.